Highly graphitized laterally interconnected SWCNT network synthesis via a sandwich-grown method

2011 J. Phys. D: Appl. Phys. 44 145401

(http://iopscience.iop.org/0022-3727/44/14/145401)

IOP PUBLISHING JOURNAL OF PHYSICS D: APPLIED PHYSICS

J. Phys. D: Appl. Phys. **44** (2011) 145401 (12pp) doi:10.1088/0022-3727/44/14/145401

Highly graphitized laterally interconnected SWCNT network synthesis via a sandwich-grown method

I-Ju Teng[1], Kai-Ling Chen[1], Hui-Lin Hsu[2], Sheng-Rui Jian[3], Li-Chun Wang[1], Jung-Hsuan Chen[4], Wei-Hsiang Wang[5] and Cheng-Tzu Kuo[1]

[1] Department of Materials Science and Engineering, National Chiao Tung University, Hsinchu 30010, Taiwan
[2] Department of Electrical and Computer Engineering, University of California, Davis, CA 95616, USA
[3] Department of Materials Science and Engineering, I-Shou University, Kaohsiung 84001, Taiwan
[4] Material and Chemical Research Laboratories, Industrial Technology Research Institute, Hsinchu 31040, Taiwan
[5] R&D Division, RITEK Corporation, Hsinchu 30316, Taiwan

E-mail: eru.mse94g@nctu.edu.tw and ctkuo@mail.nctu.edu.tw

Received 18 August 2010, in final form 17 February 2011
Published 23 March 2011
Online at stacks.iop.org/JPhysD/44/145401

Abstract

We present a sandwich-grown method for growing laterally interconnected single-walled carbon nanotube (SWCNT) networks with a high degree of graphitization by microwave plasma chemical vapour deposition (MPCVD). An Al_2O_3-supported Fe catalyst precursor layer deposited on an oxidized Si substrate with an upper Si cover is first pretreated in pure hydrogen, and then exposed to a gas mixture of methane/hydrogen for growth process at a lower growth temperature and a faster rate. The effects of various parameters, such as catalyst film thickness, gas flow rate, working pressure, growth time and plasma power, on the morphologies and structural characteristics of the SWCNT networks are investigated, and therefore provide the essential conditions for direct growth of laterally interconnected SWCNT networks. Analytical results demonstrate that the SWCNT-based lateral architecture comprises a mixture of graphene-sheet-wrapped catalyst particles and laterally interconnected nanotubes, isolated or branched or assembled into bundles. The results also show that the formation of the laterally interconnected SWCNT networks is related to the sandwich-like stack approach and the addition of an Al_2O_3 layer in the MPCVD process. The successful growth of lateral SWCNT networks provides new experimental information for simply and efficiently preparing lateral SWCNTs on unpatterned substrates, and opens a pathway to create network-structured nanotube-based devices.

(Some figures in this article are in colour only in the electronic version)

1. Introduction

Single-walled carbon nanotubes (SWCNTs) in the form of networks have displayed great potential in many applications due to their two-dimensional (2D) nanostructure and unique electrical and mechanical properties. The potential applications range from mechanically flexible systems [1–5] to high-performance devices [6–13]. Various approaches have been used for forming CNT network structures, including spin-coating [14], spraying [15], dip-coating [16], vacuum filtration [17], Langmuir–Blodgett deposition [18] and laminar flow deposition [19]. For the various above-mentioned network formation methods, a well-dispersed CNT colloidal solution and a substrate with good wettability to obtain homogeneously distributed CNT networks are highly required. In this way, the processes of sonication,

chemical treatment, centrifugation/decantation cycles and/or lithographical patterning must be applied. During these treatments, many tubes are damaged, cut and/or contaminated, which either increases the required number of CNTs or reduces/degrades the reliable electrical properties of the networks afterwards. Based on the background, direct synthesis of the CNT networks by chemical vapour deposition (CVD) becomes an appealing alternative as it requires the minimum amount of CNT processing and leaves out complex multistep solution methods into a simple one-step plasma treatment. More importantly, CVD enables extremely good control over various topological parameters, to an extent that is unlikely to be possible by solution deposition.

Jung *et al* [20] presented a thermal CVD method to build highly dense self-assembled SWCNT networks on patterned substrates (Si or SiO_2) with optimized experimental parameters, in which the growth temperature is applied in the range 800–900 °C, and the size of the transition metal particles is 3–7 nm. Yuan *et al* [21] employed Si nanocrystals decomposed from a thin silicon-on-insulator (SOI) substrate as a template to synthesize self-assembly CNT networks using Fe as a catalyst in a CVD system at 900 °C. Furthermore, Cao *et al* [2] used a Fe/Co/Mo tri-metallic and a ferritin suspension catalyst to grow metallic and semiconducting SWCNT networks on oxidized Si substrates by CVD at 840 °C and 900 °C, respectively, for active layers of thin-film transistors. In 2007, Edgeworth *et al* [22] reported two different catalyst preparation methods, sputtered Fe and ferritin, to grow SWCNT networks on SiO_2 substrates at an optimal growth temperature of 875 °C via a catalytic chemical vapour deposition (CCVD) method. Efforts so far have involved a high-temperature method with long process time to synthesize CNT networks; however, no process has been studied for the formation of highly graphitized interconnected SWCNT networks at a temperature of below 800 °C and at a faster rate, and furthermore no work has been reported for the clarification of the connection phenomenon of the CNT networks as well. It is therefore of interest to investigate a simple and reliable process for efficient growth of highly graphitized lateral SWCNT networks at a relatively lower temperature, and further identify the structure of the interconnected networks of SWCNTs.

In this study, we demonstrate a sandwich-grown method for direct growth of laterally interconnected SWCNT networks with a high degree of graphitization at a lower temperature (≦600 °C) and a faster rate by microwave plasma chemical vapour deposition (MPCVD). A detailed investigation of the effects of various parameters, such as catalyst film thickness, methane/hydrogen ratio, working pressure, growth time and plasma power, on the morphology and characteristic of the SWCNT networks is presented. In addition, the crystalline structure and average diameter distribution of the SWCNT-based lateral architecture are examined in detail. This approach offers a simple and effective way to arrive at such structures with good crystalline nature. Moreover, it opens a pathway to create network-structured nanotube-based devices without any complex multistep solubilization procedures applied.

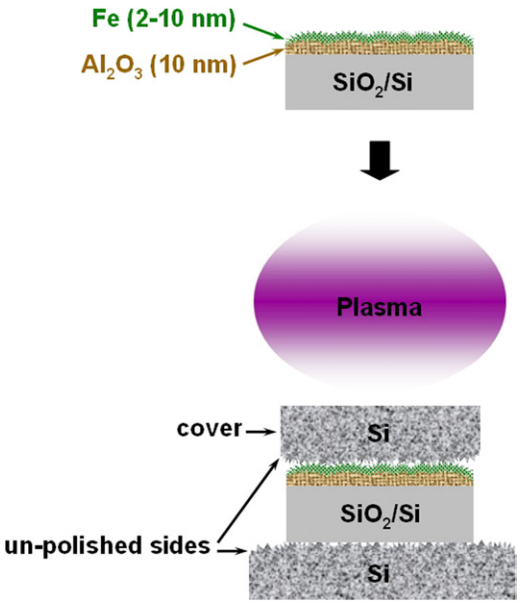

Figure 1. Schematic diagram of specimen stacking sequences.

2. Experimental

A novel sandwich-like stack approach was used for direct growth of laterally interconnected networks of SWCNTs in a MPCVD system, as shown in figure 1. A thermally oxidized silicon wafer was used as the substrate. An Al_2O_3 layer of 10 nm was deposited on the SiO_2/Si wafer first, followed by an iron (Fe) film with a thickness of 2–10 nm. Both the Al_2O_3 layer and the Fe film were prepared using direct current (dc) reactive sputtering. The Si cover used in this work was designed to suppress the ion bombardment damage of plasma on catalysts and growing tubes, and to avoid catalyst particles being poisoned easily by excess carbon species or amorphous carbon deposits. After the MPCVD system was evacuated to a base pressure of below 10^{-2} Torr by a rotary pump, hydrogen gas was then introduced at a chamber pressure of 30 Torr, forming H-plasma to heat and activate catalyst precursor layers to obtain catalyst particles. The H-plasma pretreatment conditions were as follows: plasma power of 400 W, H_2 flow rate of 100 sccm and 15 min process time. After *in situ* pretreatment, CH_4 and H_2 mixtures were introduced to initiate CNT network formation at a total pressure of 10–30 Torr and plasma power of 600–900 W for 3–8 min growth time with CH_4/H_2 ratios of 1/10 (5/50 sccm) to 0.03/10 (1.5/500 sccm). The substrate temperature was monitored to be ≦600 °C by shielded thermocouples. The morphologies and crystalline structures of the H-plasma-pretreated catalyst particles and CNT network grown samples were analysed by field-emission scanning electron microscopy (FESEM, JEOL-6500; FEI Nano SEM, Nova 200) and high-resolution transmission electron microscopy (HRTEM, JEM-2100F), respectively. A micro-Raman spectroscope (Jobin Yvon LabRam HR; Renishaw RM-1000) with a 514.5 nm (2.41 eV) laser line excitation source was employed to identify the characteristics of the as-deposited nanostructures. To obtain averaged spectra, for each sample, more than six

different locations were examined by Raman spectroscopy using an approximately 5 μm diameter laser spot. In addition, the surface morphologies of the substrate with and without Al_2O_3 deposited were observed using atomic force microscopy (AFM, VEECO DI 3100 and Asylum Research MFP-3D ORCA).

3. Results and discussion

A series of experiments were conducted to achieve highly graphitized laterally interconnected SWCNT network growth. We mainly investigated the effects of catalyst film thickness, CH_4/H_2 ratio, working pressure, growth time and plasma power on the development of SWCNT-based lateral architectures. The morphological and structural characteristics of the SWCNT networks were verified using FESEM, micro-Raman spectroscopy and HRTEM techniques.

3.1. Effect of catalyst film thickness on SWCNT network growth

Figures 2(*a*)–(*c*) show typical FESEM morphologies of the as-produced nanostructures synthesized with a CH_4/H_2 ratio of 1.5/300 sccm, chamber pressure of around 16 Torr and plasma power of 750 W for 6 min growth time, in which the insets show the SEM images of the catalyst precursor layer of various thicknesses after H-plasma pretreatment. The catalyst precursor is designed by placing 2 nm, 5 nm and 10 nm thick Fe film, respectively, on a SiO_2/Si substrate with an Al_2O_3 support layer of 10 nm. From the inserted SEM images of figures 2(*a*)–(*c*), it can be observed that under the same pretreatment conditions (H_2 flow rate of 100 sccm, chamber pressure of 30 Torr, plasma power of 400 W and 15 min process time), the morphology of the Fe particles changes from sphere to bar-like significantly, and the size of the particles becomes bigger as the thickness of the Fe film increases. With subsequent CNT growth at the selected growth parameters as mentioned above, it is found that, as a 5 nm-thick Fe precursor layer is applied, catalyst particles of suitable size are formed after H-plasma pretreatment which successfully develop laterally interconnected SWCNT networks, as displayed in figure 2(*b*). For the samples of Fe thicknesses 2 and 10 nm, however, it can be clearly seen that the as-produced nanostructure profiles differ significantly from those of the 5 nm sample. In the case of the sample with 2 nm Fe after 6 min growth time, the as-grown carbon filaments in the form of random and entangled nanotubes/fibres exhibit a relatively higher yield than those on 5 and 10 nm samples for a given area, as shown in figure 2(*a*). Since the amount of feed stock gas introduced is the same for all the samples, the observed variation in the yield of carbon filaments with various Fe thicknesses under the applied growth condition can be assigned to size-dependent catalyst activity [23–26]. In other words, in the smaller sized catalyst formed from the 2 nm Fe layer, as represented in the inset of figure 2(*a*), the diffusion length/time for carbon atoms to arrive at growth sites would become shorter, resulting in an acceleration in the growth processes of carbon filaments [23–26]. Therefore, an improved yield of carbon filaments can be obtained on the 2 nm sample under our experimental conditions. Conversely, on thickening the Fe film to 10 nm, it is likely that a thicker catalyst precursor layer is easily converted into a larger number of relatively larger Fe particles, as shown in the inset of figure 2(*c*), which consequently produce graphite-encapsulated catalyst particles with a low yield of carbon filaments growing from them on the substrate, as shown in figure 2(*c*). The result is expected for the sample with a thicker Fe layer, since in large Fe particles the diffusion length/time of carbon atoms increases which leads to a decrease in the formation rate of carbon filaments [23–26]. Furthermore, it was reported that growing a tube over larger particles formed by a thicker catalyst layer would be energetically more costly [27–29]. Therefore, it is suggested that there may not be enough energy/carbon supplied to form nucleation seeds for the growth of carbon filaments in the case of the 10 nm sample under the applied growth conditions, thus resulting in a few carbon filaments (indicated by arrows in figure 2(*c*)) with graphite-sheet-wrapped particles dominating (the particles without carbon filament growth in figure 2(*c*)) within the product. On the basis of the above SEM observations, it is suggested that the nature of carbon deposits is dependent on the catalyst particle activity, while a particularly important one is the catalyst precursor thickness dependence of laterally interconnected SWCNT network growth in our performed experiment. This is attributed to the consequences of relative rates for feedstock decomposition and migration on or through the catalysts and the energy needed for forming the SWCNT networks which are sensitive to particle size [27, 28]. The above-mentioned fact indicates a narrow growth window for the growth of laterally interconnected SWCNT networks, and according to our results the catalyst particles with suitable size formed by a 5 nm-thick Fe layer are more active and favourable for developing the networks of SWCNTs. Further studies are still needed to elucidate the nature of catalyst crystal structure and its effect on the successful growth of SWCNT-based lateral networks in this MPCVD process.

We further use Raman spectroscopy to obtain the structural information of the CNTs synthesized using 2 nm, 5 nm and 10 nm thick Fe catalyst precursor layers, as illustrated in figure 2(*d*), in which the radial breathing modes (RBMs) and sharp G-band peaks in the regions 120–350 cm^{-1} and 1550–1605 cm^{-1}, respectively, can evidently demonstrate the existence of SWCNTs [30–32]. From the RBM features in figure 2(*d*), the SWCNTs synthesized by 5 nm Fe exhibit a specific and designated diameter distribution in the resonant case of using 514.5 nm excitation, whereas the 10 nm Fe sample shows a relatively broader diameter distribution, and no RBM feature is observed in the 2 nm Fe sample. The corresponding tube diameter can also be further estimated according to the relationship between the RBM frequency and SWCNT diameter [30, 31]. On the basis of the major peaks in the range 121–183 cm^{-1} for the 5 nm Fe sample, the SWCNTs in the networks correspond to an approximate diameter distribution of around 1.35–2.11 nm. By direct comparison of the diameter distribution with a Kataura plot [30–33], it is likely that our sample has a higher portion of semiconducting SWCNTs than metallic ones. The findings

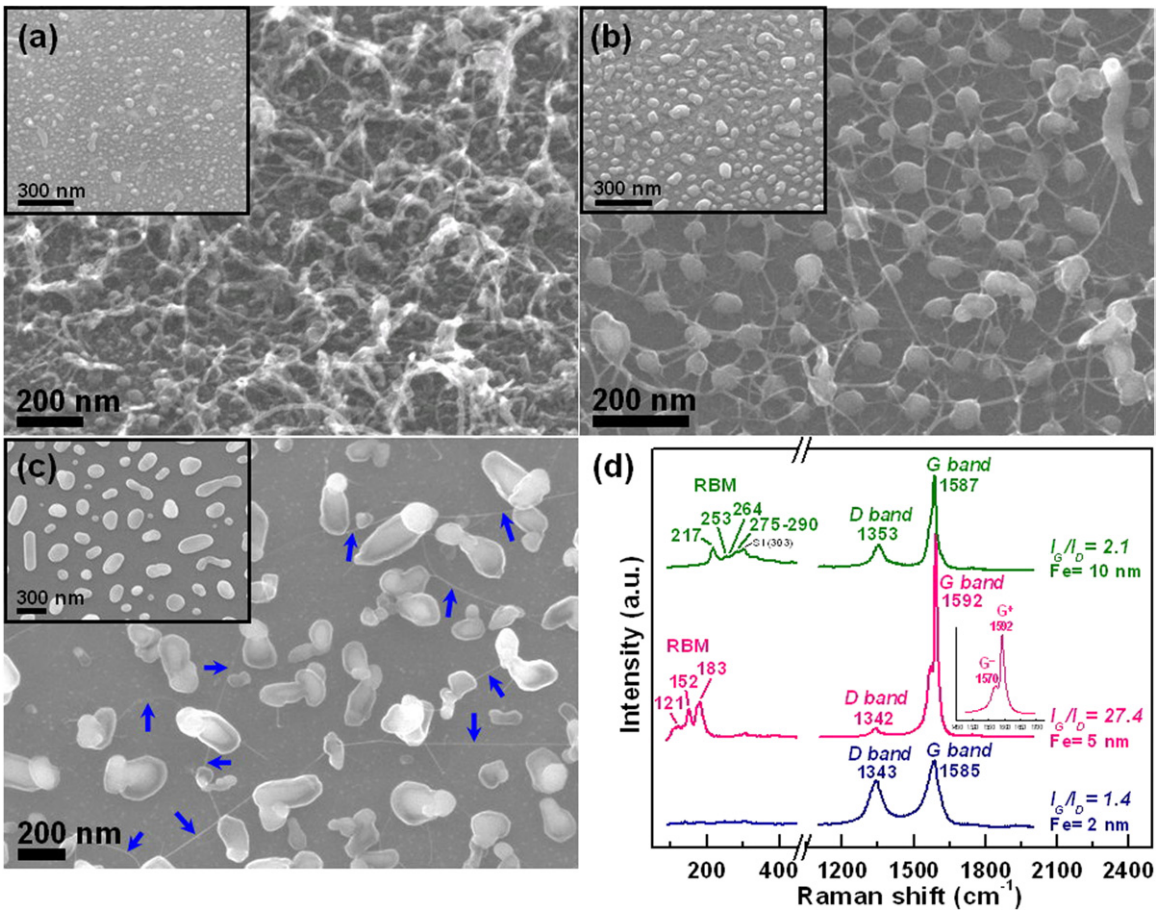

Figure 2. SEM images and Raman spectra of the CNTs grown on $Al_2O_3/SiO_2/Si$ substrates with Fe precursor films of (*a*) 2 nm, (*b*) 5 nm and (*c*) 10 nm, respectively; (*d*) the corresponding Raman spectra. The insets in (*a*), (*b*) and (*c*) show the SEM images of the H-plasma-pretreated samples (at $CH_4/H_2 = 1.5/300$ sccm, working pressure of 16 Torr and plasma power of 750 W for 6 min growth time).

on different samples of the same runs (with a total of more than 20 runs) confirm again good homogeneity of the synthesized SWCNT networks, but it is by no means intended to characterize the relative abundance of semiconducting and metallic SWCNTs as the 514.5 nm laser excitation only resonates with a fraction of SWCNTs; while it also does not allow us to conclude that the presented growth method indicates the possibility for selective synthesis of semiconducting tubes since the mechanism for preferentially growing semiconducting SWCNTs in the networks remains to be understood further. However, a previous study [34] has suggested that the relative abundances of semiconducting and metallic nanotubes do not necessarily follow the 2 : 1 ratio since various parameters and factors involved in a CVD process could be responsible for the preferential growth of a certain type of SWCNTs. Furthermore, it is of particular interest that in our recent electrical measurements, a non-linear behaviour of the I–V characteristics at low temperatures and a strong decrease in the conductivity with decreasing temperature are obtained from our SWCNT networks. The preliminary results from more than 20 devices reveal dominant features of the semiconducting nanotubes within the networks. Although we cannot currently elucidate the mechanism underlying the preferential growth phenomenon, it is believed that the successful growth of SWCNT networks with semiconducting nature does occur in our performed experiment. Further studies are currently underway to reasonably estimate the quantitative percentages of semiconducting SWCNTs in our networks, and to understand the mechanism for preferentially producing semiconducting structures in SWCNT networks. Moreover, studies on electrically characterizing devices fabricated with such SWCNT-based lateral architecture are currently underway in our group.

In addition, sample purity can be evaluated using the fitted-peak area ratio of the G-band as a characteristic of graphite to the D-band representing defects in the graphite structures, namely I_G/I_D, in the Raman spectra from CNTs to estimate the degree of crystallinity of CNTs [30–32]. A high I_G/I_D ratio demonstrates high quality of CNTs with good crystalline nature and clean parallel walls, i.e. high degree of graphitization of CNTs with little impurity/amorphous carbon, and low disorder and number of defects [30–32]. Herein, the SWCNT networks grown by the 5 nm-thick Fe exhibit superior graphitization from its considerably high I_G/I_D (=27.4) compared with those grown by 2 and 10 nm. This implies that the SWCNT networks synthesized by the 5 nm-thick Fe are of high quality, i.e. highly crystallized SWCNT networks with low disordered structures and amorphous carbon present. In addition, the two most intense G-band peaks, labelled G^+ around 1593 cm^{-1} and G^- around 1570 cm^{-1}, can be used

to distinguish between metallic and semiconducting SWCNTs through strong differences in their Raman lineshapes; of which the broadened spectral lineshape fitted by the Breit–Wigner–Fano (BWF) line is for metallic tubes, while the narrow Lorentzian lineshape is for semiconducting SWCNTs [30–32]. The observed narrow G^--band lineshape in the case of 5 nm Fe sample indicates that SWCNTs with semiconducting nature in the networks are expected. The result is highly consistent with the above RBM analysis; however, further evidence for the presence of a high percentage of semiconducting tubes in the SWCNT networks is needed and is currently under study.

To investigate the structure and diameter of the laterally interconnected SWCNT networks, we perform TEM observations of the sample grown with 5 nm thick Fe film. As can be seen in figure 3(*a*), the CNTs grow from the specific sites of particles and then connect with neighbouring particles/tubes to develop laterally interconnected networks. The situations analysed in figures 3(*b*)–(*h*) further display that the CNT-based lateral architecture comprises a mixture of graphene-sheet-wrapped catalyst particles and laterally interconnected nanotubes, isolated or branched or assembled into bundles. In addition, from figures 3(*c*)–(*e*) it can be clearly seen that the walls of the SWCNTs connect continuously with the outer layer of the graphitic shells, where the insets are low magnification images. We envision that the SWCNTs are reeled out from the graphene sheets of particles, behaving as continuous walls, and finally attach to other neighbouring particles/tubes. Additionally, the TEM images in figures 3(*f*)–(*h*) illustrate the formation of branching nanotubes during the growth. Such continuous branching nanotubes produce multiple-way junctions within our SWCNT networks. On the basis of our images it is not easy to formulate a specific/concise growth mechanism for the multi-branching SWCNT network structure. However, it is believed that structural variations must take place at the sidewalls of growing tubes and/or the growing CNT tips which then lead to the branching of CNTs [35–38]. Such variation to form branched CNTs has been explained from a topological point of view and the formation of defects [35–38]. It is considered in general that local instabilities and defects incorporated in the growing CNTs may provide a favourable/required condition for CNT branching [35–38].

It is interesting to note that there is no strong correlation between the diameter of the tubes and that of the particles (average diameter 30–100 nm in this work) for the case of our SWCNTs in networks. The result is obtained from more than 20 samples in the TEM study, of which over 20 nanotubes are observed for each sample. Although a few smaller particles encapsulated at the tip of tubes, which determines tube diameter can sporadically be found as exemplified in the circled part of the inset of figure 3(*d*), it is suggestive of particle fragmentation being likely caused by germination of dissolved carbon atoms in the bulk of catalysts during carbon growth [28] since the average size of most catalyst particles before and after carbon deposition appears in a similar range, as presented in figure 2(*b*) and its inset. Since the interconnected networks of SWCNTs synthesized by the presented growth method grow mainly from the specific sites of particles and/or branch from the growing tubes, the size of the SWCNTs is always smaller than the dimension of particles. At present, it is not completely clear about the precise nature and origin of the effects induced by our sandwich-like stack approach and the supported catalyst responsible for the formation of laterally interconnected SWCNT networks; however, the findings from this study point out that for CVD SWCNTs, the diameter of the tubes grown by the graphitization process is not always determined by the size of the particles. This is consistent with previous studies [28, 39, 40] because the final morphology and diameter of the as-synthesized carbon nanostructures are dependent not only on the growth parameters such as carbon-containing gases, temperature and gas partial pressure, but also on various factors involved in a CVD process, such as catalyst composition and catalyst support. Moreover, we carefully examine the average diameter distribution of numerous SWCNTs, and determine that for the SWCNTs in bundles the diameter is around 1.35 nm estimated from more than 100 CNTs for a single tube, whereas the diameter obtained from more than 100 isolated tubes in the TEM study is about 1.64 nm or 2.11 nm. The results are considerably close to the calculation from the frequency of the major three RBM peaks in the Raman spectra presented above. The Raman and TEM analyses demonstrate the successful growth of highly graphitized laterally interconnected SWCNT networks with a specific diameter distribution from a 5 nm-thick Fe precursor layer by the presented growth method. Therefore, it is selected as the optimum catalyst precursor thickness and employed in the experiments carried out thereafter.

3.2. *Effect of CH_4 to H_2 flow ratio on SWCNT network growth*

The CH_4 to H_2 flow ratio is another crucial parameter for the growth of SWCNT networks in this work. The morphologies of the CNTs formed with various CH_4/H_2 ratios of 1.5/300 sccm, and 5/50 sccm, 1.5/50 sccm, 1.5/100 sccm, 1.5/200 sccm, 1.5/400 sccm and 1.5/500 sccm are presented in figures 2(*b*) and 4(*a*)–(*f*), respectively, and the corresponding Raman spectra are displayed in figure 4(*g*). Other growth parameters include a working pressure of 16 Torr, growth time of 6 min and plasma power of 750 W. It can be observed from figures 4(*a*) and (*b*) that as the flow rate of CH_4 is decreased, while keeping the flow rate of H_2 constant at 50 sccm, the height of the CNT film is observed to decrease. Moreover, when the flow rate of CH_4 is maintained at 1.5 sccm, the morphology of the CNTs changes from vertically grown into surface-developed while varying the flow rate of H_2 from 50 to 100 sccm, as shown in figure 4(*c*). On further increasing the H_2 flow rate, the overall yield of the surface-grown tubes is observed to increase for the given areas, as displayed in figures 2(*b*) and 4(*d*) and (*e*). However, at the highest H_2 flow rate of 500 sccm, the yield of the laterally grown nanotubes is observed to reduce on the substrate. It is suggested that the balance between carbon deposition and etching would be shifted gradually with the variation of CH_4/H_2 ratios, which correlates with the kinetic competition between carbon and hydrogen reactive species. That is to say, the introduction of a higher CH_4 flow rate at a H_2 flow rate of 50 sccm is basically to supply more carbon sources, which enhances the

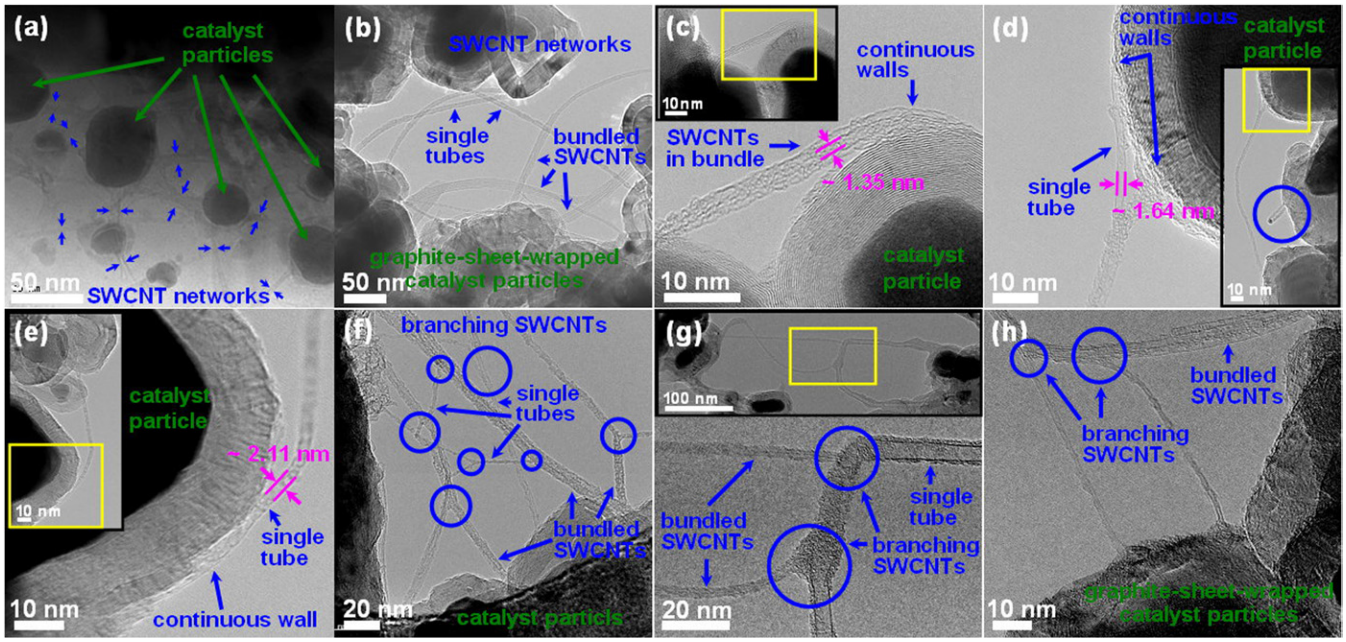

Figure 3. (*a*), (*b*) Low magnification TEM images of the SWCNT networks; (*c*)–(*e*) HRTEM images of the SWCNTs grown from the catalyst particles, where the insets are low magnification images; (*f*)–(*h*) HRTEM images of the SWCNT networks with branching structures (the circled parts).

growth rate of CNTs due to a relatively rapid saturation of catalyst particles, and thus vertical CNTs are easily formed through a pushing effect. Alternatively, increasing the H_2 flow rate at a fixed CH_4 flow rate of 1.5 sccm, the etching effect caused by reactive hydrogen species on excess carbon species and/or defect-enriched CNTs will become predominant, and thus achieve the production of 'pure' SWCNT networks with a minimum content of impurity and amorphous carbon, as shown in figures 2(*b*) and 4(*e*). Nevertheless, if a very high H_2 flow rate (such as 500 sccm) is introduced, the excess H_2 content in the plasma would excessively etch off the as-deposited carbonaceous species on the catalyst surfaces, leading to an insufficient time for carbon growth which involves surface carbon decomposition, carbon diffusion and then precipitation; hence only a low yield of SWCNTs can be collected, as displayed in figure 4(*f*). The result provides the information required for future experiments in which hydrogen must be present over a threshold amount to change the vertical structure to lateral type and then to develop SWCNT-based lateral architecture with a negligible quantity of impurity/amorphous carbon. Figure 4(*g*) compares the typical Raman spectra obtained from the CNTs grown at various CH_4/H_2 ratios. As shown, for the CH_4/H_2 ratios of 1.5/50–1.5/500 sccm, all the SWCNTs exhibit comparable graphitization and intense RBM peaks; in contrast, at the CH_4/H_2ratio of 5/50 sccm, no RBM is observed, suggesting a possible high percentage of multi-walled CNTs (MWCNTs)/carbon fibres on the sample. The main RBM peaks from different samples are located nearly at ~120–185 cm^{-1}, indicating that the SWCNTs formed at various CH_4/H_2 ratios have an approximate diameter distribution ranging from 1.34 to 2.12 nm in the resonant case of using 514.5 nm laser line excitation. It can also be found that the I_G/I_D ratio increases significantly with increasing H_2 flow rate and reaches a maximum of 31.5 at CH_4/H_2 ratio of 1.5/400 sccm, signifying that hydrogen is beneficial to keep the exposed surface clean of amorphous/disordered carbon [41], so that a weaker D-band profile can be acquired. Based on the fact that highly graphitized laterally interconnected SWCNT networks with relatively lower disordered structures/amorphous carbon present can be obtained at the CH_4 to H_2 flow ratios of 1.5/300–1.5/400 sccm, hence the CH_4/H_2 composition ratio of 1.5/300 sccm is set for MPCVD during all the experiments.

3.3. Effect of working pressure on SWCNT network growth

The influence of working pressure on the formation of SWCNT networks is explored by varying the working pressure in the range from 10 to 30 Torr under a CH_4/H_2 ratio of 1.5/300 sccm and plasma power of 750 W for 6 min growth time, as depicted in figure 2(*b*) and figures 5(*a*)–(*c*) for working pressures of 16 Torr, and 10 Torr, 23 Torr and 30 Torr, respectively. It can be found that only sparse CNTs are formed in the growth process performed at 10 Torr for a given area, while the yield of the CNTs increases dramatically as the working pressure increases. This suggests that the supply of carbon-containing sources needs to be kept high enough to enable network architecture development under the applied growth condition. At the low pressure of 10 Torr, the probability of carbon-containing molecules reacting with catalyst particles reduces due to a lower density of the carbon-containing molecules, and thus fewer catalyst particles get activated for CNT growth. On the other hand, the low operating pressure causes a low-temperature plasma as a result of the non-equilibrium state between ions, electrons and other radicals/atoms in the plasma zone, full of active species, which leads to an unsatisfactory surface energy status and an insignificant destabilization-enhanced activity for inducing CNT growth, and thus few

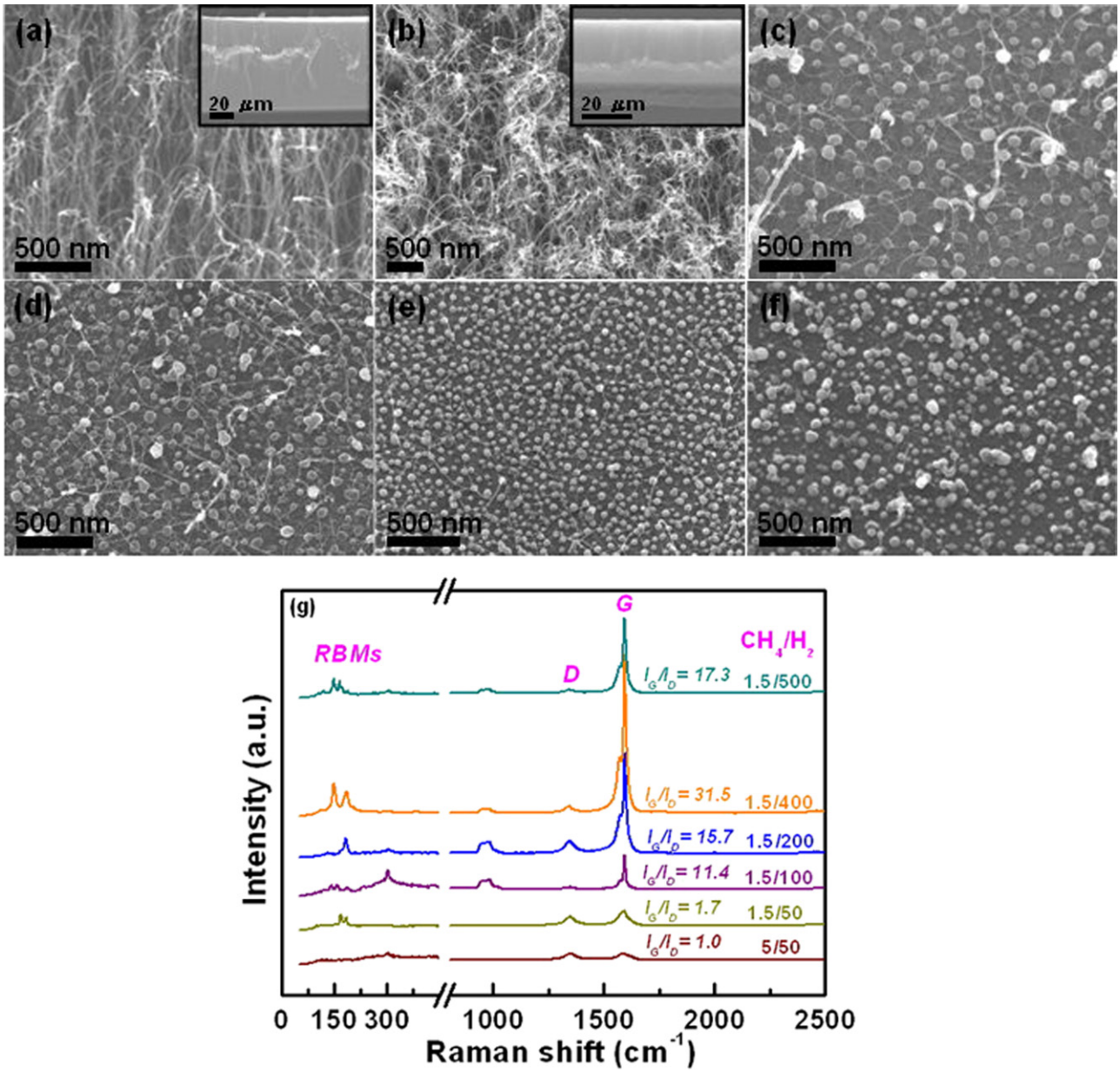

Figure 4. SEM images and Raman spectra of the CNTs grown by 5 nm-thick Fe with CH_4/H_2 ratios of (*a*) 1.5/50, (*b*) 5/50, (*c*) 1.5/100, (*d*) 1.5/200, (*e*) 1.5/400 and (*f*) 1.5/500 sccm, respectively; (*g*) the corresponding Raman spectra (at working pressure of 16 Torr and plasma power of 750 W for 6 min growth time).

carbon filaments can be grown on the substrate, as shown in figure 5(*a*). As the working pressure is increased, the reactive species concentration in the chamber is adjusted, which means that the number of collisions between gas molecules and the catalyst surface is increased proportionally [42–44]. That is to say, when the CVD process is carried out at higher working pressures, more carbon-containing molecules interact with the catalyst particles [42–44]. As a result, more catalyst particles get activated for CNT growth, and this leads to an improved yield of SWCNTs in the networks [42–44], as shown in figure 2(*b*), and figures 5(*b*) and (*c*) for pressures varied from 16 to 30 Torr. The pressure dependence indicates a correlation between the number of activated catalyst particles and the concentration of supplied carbon atoms, and also implies that by changing the working pressure in a controllable manner, the yield of SWCNTs in the networks can be manipulated. It is important as different electrical applications require different morphologies and quantities. The Raman spectra from the samples grown at different pressures are illustrated in figure 2(*d*) and figure 5(*d*) for working pressures of 16 Torr, and 10 Torr, 23 Torr and 30 Torr, respectively. It is noted that the samples grown with the working pressure in the range 16–30 Torr exhibit strong RBM peaks and extremely weak D bands, indicating the existence of highly graphitized SWCNT networks with low disordered structures and/or little amorphous carbon present. In addition, based on the similar ratio of I_G/I_D obtained from the growth process performed at 16–30 Torr working pressures, we suggest that more carbon-containing molecules in a higher working pressure process are consumed mainly by the generated active sites to nucleate

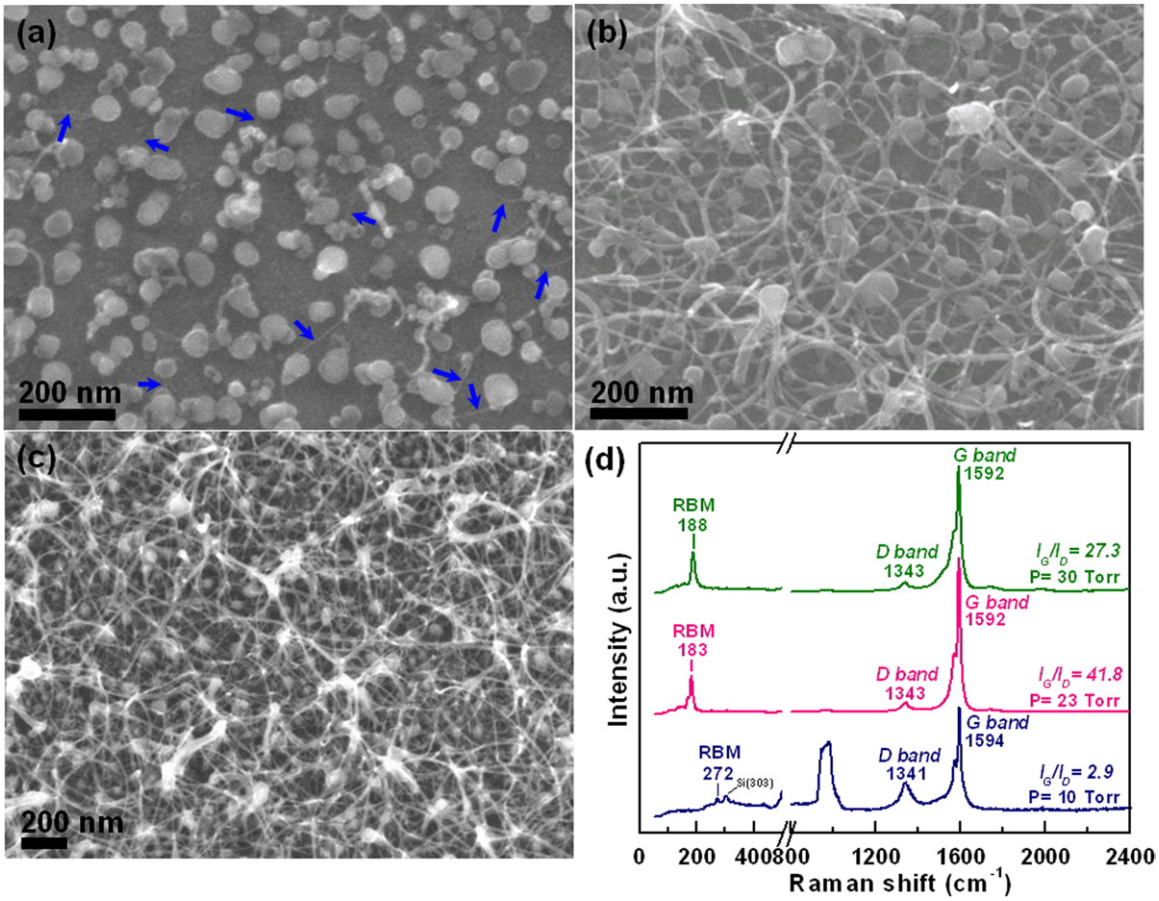

Figure 5. SEM images and Raman spectra of the CNTs grown by 5 nm-thick Fe at working pressures of (*a*) 10 Torr, (*b*) 23 Torr and (*c*) 30 Torr, respectively; (*d*) the corresponding Raman spectra (at CH_4/H_2 =1.5/300 sccm and plasma power of 750 W for 6 min growth time).

CNTs rather than causing the accumulation of amorphous carbon structure. In addition, the observed frequencies of the RBM peaks for the growth process performed at 23–30 Torr working pressures correspond to SWCNT diameters in the range 1.31–1.35 nm in the resonant case of using 514.5 nm line of Ar laser for excitation. The investigations of the effect of working pressure on SWCNT network growth provide useful information in designing CVD processes for manipulating the production of SWCNTs in networks for various desired device applications.

3.4. Effect of growth time on SWCNT network growth

The effect of varying the growth time on the resulting SWCNT networks is given in figure 2(*b*) and figures 6(*a*)–(*c*) for growth times of 6 min, and 3 min, 4 min and 8 min, respectively, while keeping the CH_4/H_2 ratio, working pressure and plasma power at 1.5/300 sccm, 16 Torr and 750 W, respectively. As shown in figure 6(*a*), at the growth time of 3 min, only a few lateral CNTs connect with their neighbouring particles for a given area, while at 4 min, figure 6(*b*), more particles are linked together by growing CNTs. Increasing the growth time is likely to increase the quantity of interconnected CNTs; however, as the continuous growth time is extended to 8 min, SWCNT-based lateral architecture is developed but with agglomerated particles and a significant number of MWCNTs among the networks as displayed in figure 6(*c*). The possible reason is that when the growth time increases, carbon-containing gas decomposes and diffuses into active catalyst particles, while hydrogen continuously keeps the surface clean of carbon and prevents catalyst deactivation for CNT growth. If the growth time is very long, catalyst particles are inclined to aggregate, and more defective carbon filaments/amorphous carbon structures get accumulated as a result of sufficient plasma heating. Accordingly, the growth of a large number of bended/entangled carbon filaments and the assembly of catalyst particles at 8 min growth time, as presented in figure 6(*c*), illustrates the result of long time formation in the MPCVD process. Thus, 6 min is considered to be the optimum growth time for synthesizing laterally interconnected SWCNT networks with a negligible quantity of agglomerated particles and MWCNTs/carbon fibres in our performed experiment, as shown in figure 2(*b*). The corresponding Raman spectra of the as-deposited samples for growth times of 3, 4 and 8 min are shown in figure 6(*d*). The RBM signals from the CNTs grown at 4 min and 8 min are observed in the frequency ranges 121–185 cm^{-1} and 184–205 cm^{-1}, respectively, which are indicative of the SWCNTs having an approximate diameter distribution of 1.34–2.11 nm in 4 min networks and 1.20–1.34 nm in 8 min networks in the resonant case of using 514.5 nm laser line excitation. Although more defects and disordered graphitic material are present for the extended

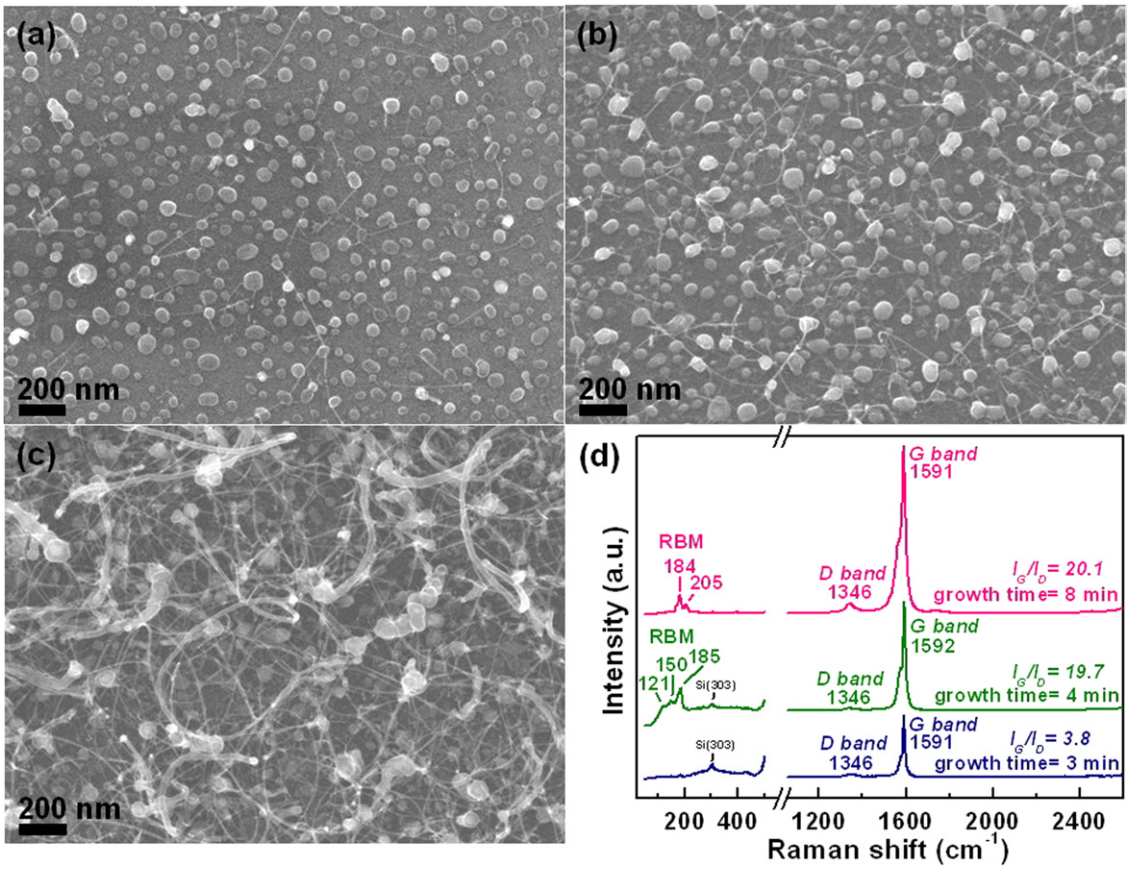

Figure 6. SEM images and Raman spectra of the CNTs grown by 5 nm-thick Fe at growth times of (*a*) 3 min, (*b*) 4 min and (*c*) 8 min, respectively; (*d*) the corresponding Raman spectra (at $CH_4/H_2 = 1.5/300$ sccm, working pressure of 16 Torr and plasma power of 750 W).

growth time of 8 min, as indicated by the slightly larger, more structured D peak, consistent with figure 6(*c*), the observed high I_G/I_D ratios for the growth time of 4–8 min still evidence the growth of highly graphitized SWCNT networks. The growth time studies show that the presented growth method represents a more efficient way to prepare SWCNT-based lateral networks on substrates directly.

3.5. Effect of plasma power on SWCNT network growth

The effect of plasma power on the growth of SWCNT networks is also studied. Figures 7(*a*) and (*b*) display the CNTs synthesized at plasma powers of 600 W and 900 W, respectively. For the study, CNT growth is carried out at a CH_4/H_2 ratio of 1.5/300 sccm and working pressure of 16 Torr for 6 min. Referring to figures 2(*b*), and 7(*a*) and (*b*), the production of CNTs in the networks generally increases with increasing plasma power for given areas. In general, a microwave plasma operating at a low power is a low-temperature plasma which will lead to a lower plasma decomposition rate of hydrogeneous and carbonaceous gases, and thus result in a lower tube growth rate. The sparse tube appearance at the lower plasma power condition of 600 W may be due to insufficient temperature in the plasma space for rapidly generating reactive species for CNT growth within the selected growth time. As the plasma power is increased up to 750 W or even to 900 W, the higher introduced plasma power can not only ionize more gases but also cause local surface heating, leading to a situation where plenty of carbon species reach the catalyst particles, followed by a CNT growth procedure to carry out the formation of laterally interconnected SWCNT networks. Further comparing the 750 W sample with the 900 W sample, it is obvious that a relatively higher plasma power process is likely to result in the formation of many large-sized carbon filaments over the substrate as shown in figure 7(*b*). This is because the increased temperature and reactant gases' decomposition rate resulting from the relatively higher plasma power supply will promote more surface instability on the catalyst particles and/or nanotubes, and therefore induce more active nucleation sites for the formation of CNTs. It is concluded that for the presented growth method, the microwave power of 750 W is the optimum plasma level to grow interconnected networks of SWCNTs with a negligible quantity of MWCNTs/carbon fibres in our performed experiment. Figure 7(*c*) shows the Raman spectra of the as-grown samples synthesized at plasma powers of 600 W and 900 W, respectively. The high I_G/I_D ratio (=24.3) and RBM peaks confirm the formation of SWCNT networks with a high degree of graphitization on the 900 W plasma power sample. The observed frequency range of the RBM signals corresponds to the SWCNTs in the networks with a diameter distribution of about 0.99–1.65 nm in the resonant case of using 514.5 nm excitation. Whereas the very weak RBM density at 173 cm^{-1} and the low ratio of the intensity of G peak to D peak

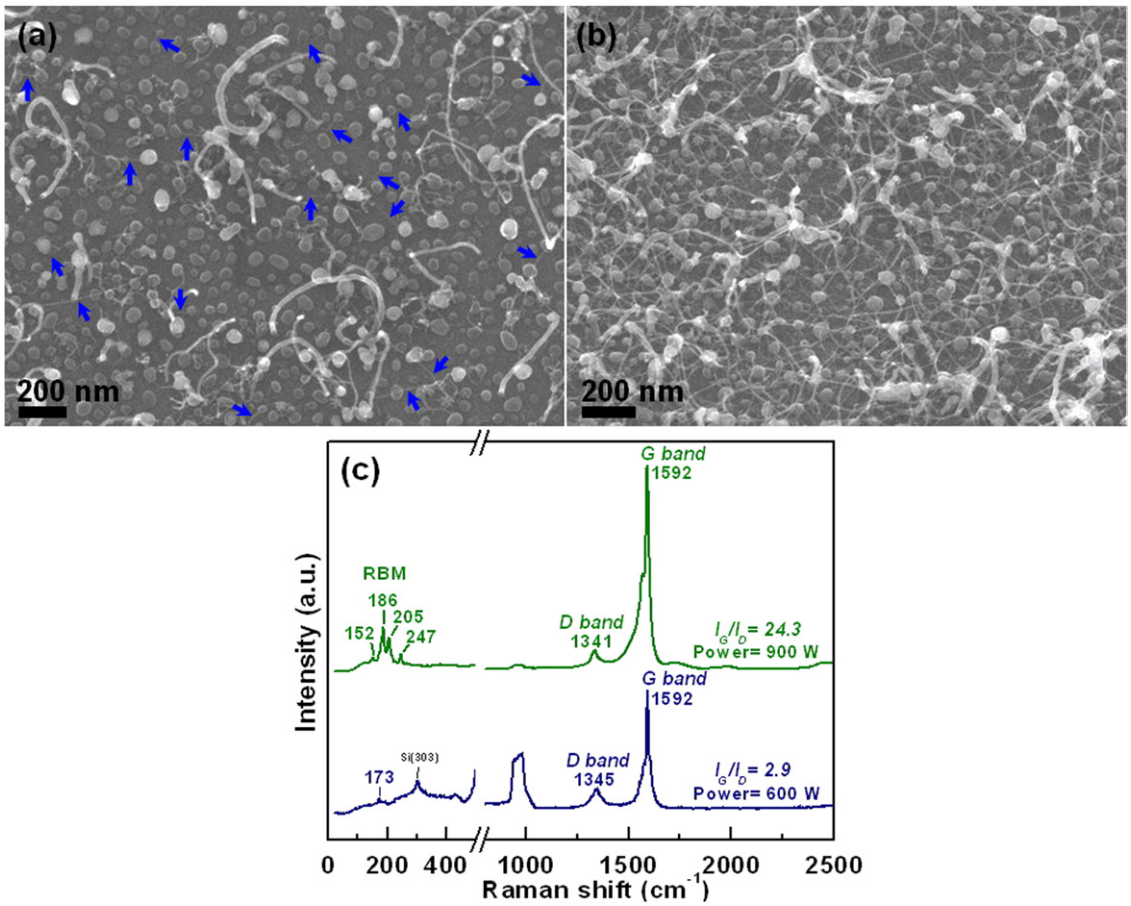

Figure 7. SEM images and Raman spectra of the CNTs grown by 5 nm-thick Fe at plasma powers of (*a*) 600 W and (*b*) 900 W, respectively; (*c*) the corresponding Raman spectra (at $CH_4/H_2 = 1.5/300$ sccm, working pressure of 16 Torr and growth time of 6 min).

obtained from the 600 W sample suggest the existence of a low yield of SWCNTs and the presence of a higher proportion of sp^3-like carbon on the substrate.

From the FESEM, HRTEM images and Raman spectroscopy mentioned above, we can thus conclude as follows: the interconnected SWCNT networks synthesized by a sandwich-grown method in this work are surface-grown and of good crystalline nature. By the presented growth method and at the selected growth parameters, a 5 nm-thick Fe precursor layer supported by an Al_2O_3 layer is proven to be the optimum catalyst precursor to form the SWCNT-based lateral architecture. Furthermore, higher H_2 flow rate basically results in lower impurity and/or amorphous structure among the networks at a fixed amount of CH_4 content of 1.5 sccm, i.e. the degree of graphitization of SWCNT networks is enhanced with lowering CH_4/H_2 ratio, and it reaches a maximum at the CH_4/H_2 ratio of 1.5/400 sccm. By increasing the working pressure in a controllable manner the yield of the SWCNTs in the networks can be altered for future desired applications. In addition, very long growth duration and high plasma power will favour the aggregation of catalyst particles and the accumulation of bended/entangled carbon filaments/amorphous carbon structures over the samples as a result of the higher temperature and more active species generated in the plasma. Thus the optimum conditions for growing highly graphitized laterally interconnected SWCNT networks with a negligible quantity of large-sized carbon filaments are growth time of 6 min and plasma power of 750 W.

3.6. Effect of specimen stacking and Al_2O_3 support layer on SWCNT network growth

Explanations of the fundamental growth mechanism of the sandwich-grown method as proposed in figure 1 are still a bit speculative; however, the following observations may shed some light on some indispensable factors responsible for the formation of laterally interconnected SWCNT networks in this work. We first consider the effect of specimen stacking on the growth of SWCNT networks. We perform SEM observation of a sample in direct contact with the microwave plasma without an upper Si cover throughout the CNT growth process, as shown in figure 8(*a*), in which the inset reveals the schematic of the specimen position with respect to the plasma. The growth is performed with CH_4/H_2 of 1.5 sccm/300 sccm flow rate at 16 Torr working pressure and 750 W plasma power for 6 min. As seen in the figure, only chain-like/agglomerated deposits containing carbon are observed on the substrate. The result confirms that if the catalyst particles are in direct contact with the microwave plasma, the selected growth parameters are unfavourable for CNT growth. In other words, the sandwich-like stack approach plays one of the determinant roles in nucleating SWCNTs and then forming the interconnected network architecture.

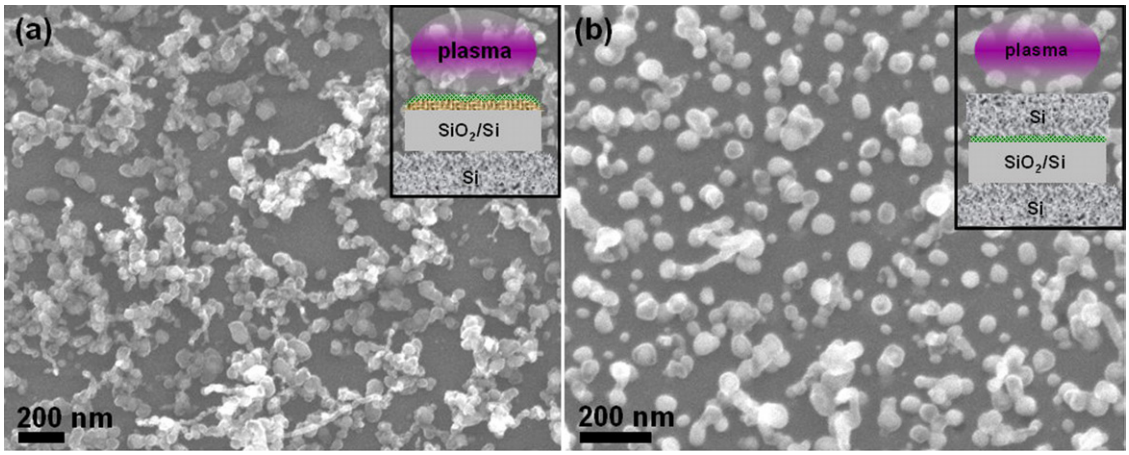

Figure 8. SEM images of (*a*) the carbon nanostructures formed on a substrate in direct contact with the microwave plasma without an upper Si cover, and (*b*) the carbon nanostructures formed on a substrate without Al_2O_3 as a support layer (at $CH_4/H_2 = 1.5/300$ sccm, working pressure of 16 Torr, plasma power of 750 W and growth time of 6 min). The insets in (*a*) and (*b*) show the schematic of the specimens.

Another important result in our experiment is the strong dependence of the SWCNT networks grown on an Al-based support layer. We prepare a substrate without Al_2O_3 between the catalyst precursor film and the substrate for this MPCVD process. By conducting a comparative SEM study we find that the morphologies after growth on a plain SiO_2 surface and on an Al_2O_3 layer are obviously different, as displayed in figures 8(*b*) and 2(*b*). The inset in figure 8(*b*) shows the schematic of a specimen that has undergone the process with the same parameters without an Al_2O_3 layer. Without the use of an Al_2O_3 support layer, SWCNT networks cannot form under the applied growth conditions. One possible explanation involves the stability difference in the two oxide layers. By comparing the heat of formation for Al_2O_3 and SiO_2, we note that $Al_2O_3$is an extremely stable oxide since its heat of formation ($-1675.7\,\mathrm{kJ\,mol^{-1}}$) is much larger than that of SiO_2 ($-910.7\,\mathrm{kJ\,mol^{-1}}$) [45]. It is suggested that the catalytic activity of Fe may be partially poisoned by a reaction/interaction between Fe and the support layer [45, 46]. The poisoning effect should be more severe on SiO_2 due to the relatively lower stability compared with that of Al_2O_3, resulting in a difficulty in growing CNTs on the SiO_2/Si under the applied growth conditions [45, 46]. Furthermore, the roughness of the catalyst support layer could be another factor affecting SWCNT growth [47–50]. It is reported that the introduction of the Al-based catalyst support layer between the substrate and the catalyst leads to the appearance of more active nucleation sites on the catalyst surface for carbon atoms to reach and further for nanotubes to grow, and also improves the diffusion of reactant gases to the catalyst clusters due to an increase in surface roughness/porosity [47–50]. As also confirmed by our AFM measurements, the RMS value of roughness of the Al_2O_3 surface present is about 1 nm, which is indeed higher than 0.27 nm for the SiO_2 case. The above investigations imply that Al_2O_3 in our case could not only prevent the catalysts from reacting with the SiO_2 surface, but also provide more active nucleation sites to catalyse SWCNT growth. As the studies reported here indicate, both the sandwich-like stack approach and the Al_2O_3 support layer are important contributing factors towards obtaining SWCNT networks under our experimental conditions. However, details of the formation mechanism of the laterally interconnected SWCNT networks and the key role played by the applied sandwich-like stack approach and the catalyst support material for producing the SWCNT networks in this MPCVD process need further verification.

4. Conclusions

In summary, direct growth of highly graphitized laterally interconnected SWCNT networks by a MPCVD process is demonstrated at a lower growth temperature ($\leqq$600 °C) and a faster rate using a sandwich-grown method with an upper Si cover and a 5 nm-thick Fe layer supported by a 10 nm Al_2O_3 layer deposited on a SiO_2/Si substrate. A detailed examination of the effects of various parameters on the formation of SWCNT networks is also presented. The yield of SWCNTs in the networks for a given area can be altered by varying the growth parameters. The result is important as different electrical applications require different morphologies and quantities. The preferential growth of highly graphitized laterally interconnected SWCNT networks with little impurity/amorphous carbon, and low disorder and number of defects is accomplished at a CH_4/H_2 ratio of 1.5/300–1.5/400 sccm, working pressure of $\geqq$16 Torr, growth time of 6 min and plasma power of 750 W. The HRTEM investigations show that the SWCNT-based lateral architecture consists of a mixture of graphene-sheet-wrapped catalyst particles and laterally interconnected nanotubes, isolated or branched or assembled into bundles, in which the average diameter distribution of the SWCNTs is around 1.35 nm for the tube in a bundle and 1.64 nm or 2.11 nm for an isolated tube under the applied growth conditions. In addition, the sandwich-like stack approach and Al_2O_3 support layer have demonstrated to be indispensable factors responsible for the generation of SWCNT networks in this MPCVD process. However, further studies are needed to elucidate the mechanism for the formation of such SWCNT-based

lateral architecture and to clarify the key role played by various factors involved in this MPCVD process for the successful growth of SWCNT networks. The morphological and structural characterizations of the SWCNT networks have immediate and immense implications for the development of network-structured nanotube-based electronic systems and diverse sensing devices, especially signifying a simple and efficient SWCNT network synthesis process and opening new possibilities for direct device integration.

Acknowledgments

The authors acknowledge the financial support from the National Science Council of Taiwan under contract Nos NSC98-2221-E-451-001 and NSC97-2112-M-214-002-MY2. The authors would also like to acknowledge the facility support from the Materials Science and Engineering Department, Center for Nano Science and Technology and Nano Facility Center at National Chiao Tung University, and Nanomaterials in the Environment, Agriculture, and Technology Organized Research Unit (NEAT-ORU) at UC Davis and RITEK Corporation.

References

[1] Bradley K, Gabriel J C P and Gruner G 2003 *Nano Lett.* **3** 1353
[2] Cao Q, Hur S H, Zhu Z T, Sun Y G, Wang C J, Meitl M A, Shim M and Rogers J A 2006 *Adv. Mater.* **18** 304
[3] Zhou Y, Gaur A, Hur S H, Kocabas C, Meitl M A, Shim M and Rogers J A 2004 *Nano Lett.* **4** 2031
[4] Zhang D, Ryu K, Liu X, Polikarpov E, Ly J, Tompson M E and Zhou C 2006 *Nano Lett.* **6** 1880
[5] Wu Z C *et al* 2004 *Science* **305** 1273
[6] Novak J P, Snow E S, Houser E J, Park D, Stepnowski J L and McGill R A 2003 *Appl. Phys. Lett.* **83** 4026
[7] Vichchulada P, Zhang Q and Lay M D 2007 *Analyst* **132** 719
[8] Byon H R and Choi H C 2006 *J. Am. Chem. Soc.* **128** 2188
[9] Gui E L *et al* 2007 *J. Am. Chem. Soc.* **129** 14427
[10] Li J and Zhang S L 2009 *Phys. Rev.* B **79** 155434
[11] Rowell M W, Topinka M A, McGehee M D, Prall H J, Dennler G, Sariciftci N S, Hu L and Gruner G 2006 *Appl. Phys. Lett.* **88** 233506
[12] Barnes T M, Wu X, Zhou J, Duda A, van de Lagemaat J, Coutts T J, Weeks C L, Britz D A and Glatkowski P 2007 *Appl. Phys. Lett.* **90** 243503
[13] Ong P L, Euler W B and Levitsky I A 2010 *Nanotechnology* **21** 105203
[14] Meitl M A, Zhou Y X, Gaur A, Jeon S, Usrey M L, Strano M S and Rogers J A 2004 *Nano Lett.* **4** 1643
[15] Bekyarova E, Itkis M E, Cabrera N, Zhao B, Yu A, Gao J and Haddon R C 2005 *J. Am. Chem. Soc.* **127** 5990
[16] Jang E Y, Kang T J, Im H W, Kim D W and Kim Y H 2008 *Small* **4** 2255
[17] Lim C, Min D H and Lee S B 2007 *Appl. Phys. Lett.* **91** 243117
[18] Kim Y, Minami N, Zhu W, Kazaoui S, Azumi R and Matsumoto M 2003 *Japan. J. Appl. Phys.* **42** 7629
[19] Zhang Q, Vichchulada P, Cauble M A and Lay M D 2009 *J. Mater. Sci.* **44** 1206
[20] Jung Y J, Homma Y, Ogino T, Kobayashi Y, Takagi D, Wei B, Vajtai R and Ajayan P M 2003 *J. Phys. Chem.* B **107** 6859
[21] Yuan H C, Yang B, Simmons J M, Marcus M S, Ma Z, Eriksson M A and Lagally M G 2005 *Proc. SPIE* **5971** 597118
[22] Edgeworth J P, Wilson N R and Macpherson J V 2007 *Small* **3** 860
[23] Patole S P, Kim H, Choi J, Kim Y, Baik S and Yoo J B 2010 *Appl. Phys. Lett.* **96** 094101
[24] Jang Y T, Ahn J H, Lee Y H and Ju B K 2003 *Chem. Phys. Lett.* **372** 745
[25] Wei Y Y, Eres G, Merkulov V I and Lowndes D H 2001 *Appl. Phys. Lett.* **78** 1394
[26] Choi Y C, Shin Y M, Lee Y H, Lee B S, Park G S, Choi W B, Lee N S and Kim J M 2000 *Appl. Phys. Lett.* **76** 2367
[27] Dai H J, Rinzler A G, Nikolaev P, Thess A, Colbert D T and Smalley R E 1996 *Chem. Phys. Lett.* **260** 471
[28] Yu Z, Chen D, Tøtdal B and Holmen A 2005 *J. Phys. Chem.* B **109** 6096
[29] Hafner J H, Bronikowski M J, Azamian B R, Nikolaev P, Rinzler A G, Colbert D T, Smith K A and Smalley R E 1998 *Chem. Phys. Lett.* **296** 195
[30] Jorio A, Pimenta M A, Souza Filho A G, Saito R, Dresselhaus G and Dresselhaus M S 2003 *New J. Phys.* **5** 139 (and references therein)
[31] Dresselhaus M S, Dresselhaus G, Satio R and Jorio A 2005 *Phys. Rep.* **409** 47 (and references therein)
[32] Dresselhaus M S, Dresselhaus G, Jorio A, Souza Filho A G and Saito R 2002 *Carbon* **40** 2043
[33] Kataura H, Kumazawa Y, Maniwa Y, Umezu I, Suzuki S, Ohtsuka Y and Achiba Y 1999 *Synth. Met.* **103** 2555
[34] Li Y *et al* 2004 *Nano Lett.* **4** 317
[35] Ting J M and Chang C C 2002 *Appl. Phys. Lett.* **80** 324 (and references therein)
[36] Charlier J C 2002 *Acc. Chem. Res.* **35** 1063
[37] Xue B, Shao X and Cai W 2008 *Comput. Mater. Sci.* **43** 531
[38] Fu D, Zeng X, Zou J, Qian H, Li X and Xiong X 2009 *Mater. Chem. Phys.* **118** 501
[39] Matthews K D, Lemaitre M G, Kim T, Chen H, Shim M and Zuo J M 2006 *J. Appl. Phys.* **100** 044309
[40] Loiseau A, Gavillet J, Ducastelle F, Thibault J, Stéphan O, Bernier P and Thair S 2003 *C. R. Phys.* **4** 975
[41] Ferrari A C and Robertson J 2000 *J. Phys. Rev.* B **61** 14095
[42] Pint C L, Nicholas N, Pheasant S T, Duque J G, Parra-Vasquez A N G, Eres G, Pasquali M and Hauge R H 2008 *J. Phys. Chem.* C **112** 14041
[43] Zhang R, Tsui R K, Tresek J, Rawlett A M, Amlani I, Hopson T and Fejes P 2003 *J. Phys. Chem.* B **107** 3137
[44] Li W Z, Wen J G, Tu Y and Ren Z F 2001 *Appl. Phys.* A **73** 259
[45] Bae E J, Min Y S, Kim U and Park W 2007 *Nanotechnology* **18** 015601 (and references therein)
[46] Zhou W, Ding L and Liu J 2009 *Nano Res.* **2** 593 (and references therein)
[47] Delzeit L, Chen B, Cassel A, Stevens R, Nguyen C and Meyyappan M 2001 *Chem. Phys. Lett.* **348** 368
[48] La M K, Mohamed N M and Begam K M 2008 *Adv. Mater. Res.* **32** 29
[49] Seidel R, Duesberg G S, Unger E, Graham A P, Liebau M and Kreupl F 2004 *J. Phys. Chem.* B **108** 1888
[50] Hart A J, Slocum A H and Royer L 2006 *Carbon* **44** 348